TREATMENT OF REFRACTIVITY FLUCTUATIONS BY FULLY POPULATED VARIANCE-COVARIANCE MATRICES

Steffen Schön [(1)], Fritz K. Brunner[(2)]

[(1)] Institut für Erdmessung (IfE), Leibniz Universität Hannover Schneiderberg 50, D-30167 Hannover, Germany
Email: schoen@ife.uni-hannover.de

[(2)] Institute for Engineering Geodesy and Measurements Systems (EGMS), Graz University of Technology
Steyrergasse 30, A-8010 Graz, Austria
Email: fritz.brunner@TUGraz.at

INTRODUCTION

The incomplete knowledge of the atmospheric composition and dynamics along the signal path is still an accuracy limitation for GNSS-based parameter estimation. In fact, the dynamic processes in the atmosphere induce correlated wave propagation effects on GNSS signals. Usually, these correlations are not modelled in the variance-covariance-matrix (VCM) of the observations. Hence, too optimistic uncertainty measures are obtained for GNSS derived parameters like point positions or estimated zenith wet delays.

Refractivity fluctuations in the troposphere are a prominent example for sources for such physical correlations. Based on turbulence theory, the authors have proposed the structure of a VCM that adequately explains such correlations. The magnitudes of the VCM elements depend not only on the satellite-antenna geometry (expressed by the station separation, the azimuths and elevation angles of the satellites) but also on the prevailing atmospheric conditions. The latter ones can be parameterised, e.g. by the wind velocity and direction, the so-called structure constant of the refractivity, C_n^2, and the outer scale length, L_0. In this paper, we analyse how the wind velocity and direction influence the structure of our VCM and the correlation and decorrelation processes reflected in the VCM.

MATHEMATICAL DESCRIPTION OF VARIANCES AND COVARIANCES INDUCED BY REFRACTIVITY FLUCTUATIONS

Turbulence theory [1] provides suitable concepts to mathematically handle the random fluctuations of the refractivity and their impact on phase measurements of space geodetic microwave techniques like Very Long Baseline Interferometry (VLBI) or Global Navigation Satellite Systems (GNSS, e.g., GPS GLONASS or Galileo). In the lower atmosphere, the integration of the refractivity (steady-state part) along the lines-of-sight leads to the slant tropospheric delays. The refractivity fluctuations yield random phase fluctuations which can be assessed by a fully populated VCM. In addition, this matrix can be interpreted as the VCM of the tropospheric slant delays.

A common-used approach for the formulation of such a VCM of the tropospheric delays is the integration of the refractivity structure function D_n along the lines-of-sight, cf. [2] for the VLBI configuration. For an overview on the subsequent work which is based on this approach refer to [3]. In our development [4] however, we start with a description of the spectrum of refractivity fluctuation yielding a more general description than the structure function-based approach. In the following we briefly summarize our developments of a VCM for GPS phase observations induced by refractivity fluctuations. For more details please refer to [4]

We use the von Karman spectrum to express the spectrum of refractivity fluctuations Φ_n [1, p.30ff]. It is mathematically more convenient than the initial formulation of the spectrum by Kolmogorov since it avoids singularities for $\kappa \to 0$.

$$\Phi_n(\kappa) = \frac{0.033\, C_n^2}{\left(\kappa^2 + \kappa_0^2\right)^{11/6}} \sim \kappa^{-11/3}, \quad 0 < \kappa < \kappa_S, \tag{1}$$

where κ denotes the wavenumbers, $\kappa_0 = 2\pi / L_0$ is the wave number corresponding to the outer scale lengths L_0, and C_n^2 the structure constant of refractivity that expresses the strength of the turbulence. From Kolmogorov's dimensional

analysis [1, p.37ff] it is known that for the inertial subrange which is bounded by L_0 and $l_0 = 2\pi / \kappa_S$ a spectral index $\nu = -11/3$ holds.

Since the turbulent medium is far to be a homogeneous and isotropic random medium as implicitly assumed in (1), we have to extend this representation twice: (i) Using a 3d spectrum inhomogeneities are taken into account. (ii) In a first approximation anisotropy is considered by introducing a different scaling of each of the three wavenumbers yielding so-called scratched wavenumbers, cf. [4].

The integration of the refractivity variations along the lines-of-sight allows to relate the spectrum of refractivity expressed by the Fourier wavenumber decomposition [1, p.136ff] to the phase covariances between two points A and B which equals the covariances of the tropospheric delays. For the most general case, the covariance between the GNSS phase observation $\varphi_A^i(t_A)$ from station A to satellite *i* at epoch t_A and the phase observation $\varphi_B^j(t_B)$ from station B to satellite *j* at epoch t_B reads

$$\left\langle \varphi_A^i(t_A),\ \varphi_B^j(t_B) \right\rangle = \int_0^\infty \int_0^\infty \int_{-\infty}^\infty \int_{-\infty}^\infty \int_{-\infty}^\infty \Phi_n\left(\boldsymbol{\kappa}, \frac{\mathbf{r}_A^i + \mathbf{r}_B^j}{2}\right) e^{i\,\boldsymbol{\kappa}^T \mathbf{d}}\, \mathbf{d}^3\boldsymbol{\kappa}\, ds_1 ds_2 \tag{2}$$

where

$$\mathbf{d} = \mathbf{r}_B^j(ds_2) + \boldsymbol{\rho}_A^B - \mathbf{v}\,\Delta t - \mathbf{r}_A^i(ds_1) \tag{3}$$

denotes the vector separating the integration points, $\mathbf{r}_A^i, \mathbf{r}_B^j$ the vectors of lines-of-sight between the station A and the satellite *i*, and the station B and the satellite *j*, respectively. The vector $\boldsymbol{\rho}_A^B$ gives the station separation (baseline), and ds_1, ds_2 are the integration increments along the lines-of-sight. The 3d vector of wavenumbers is denoted by $\boldsymbol{\kappa}$.

Temporal correlations are taken into account using Taylor's hypothesis of frozen turbulence, cf. [1, p.240ff], i.e. by assuming that the turbulent variations travel in wind direction with the constant wind velocity v > 0. This constant wind vector is parameterized in a topocentric coordinate system as:

$$\mathbf{v} = v\left(\cos A \cos E \quad \sin A \cos E \quad \sin E\right)^T, \tag{4}$$

where *A*, *E* denote the wind direction in azimuth and elevation. Since the model (2) is based on the separation distance of the integration points, the temporal separation $\Delta t = t_B - t_A$ of two measurements is transformed in a spatial separation by multiplication with the wind velocity vector $\boldsymbol{\Lambda} = \mathbf{v}\,\Delta t$ see [1, p.49, 162ff] for a detailed discussion.

The integrations in (2) about the three wavenumbers can be solved analytically [4], yielding

$$\left\langle \varphi_A^i(t_A),\ \varphi_B^j(t_B) \right\rangle = \frac{12}{5} \frac{0.033}{\Gamma\left(\frac{5}{6}\right)} \frac{\sqrt{\pi^3}\,\kappa_0^{-2/3} 2^{-1/3}}{\sin\varepsilon_A^i \sin\varepsilon_B^j} C_n^2 \int_0^H \int_0^H \left(\kappa_0 d\right)^{1/3} K_{-1/3}\left(\kappa_0 d\right) dz_1 dz_2 \tag{5}$$

where Γ denotes the gamma function and *K* the modified Bessel function of second kind (MacDonald function), [5]. The integration along the slant lines-of-sight is changed in an integration with height, which enters the elevation angles $\varepsilon_A^i, \varepsilon_B^j$ of the satellites and the vertical increments dz_1, dz_2. The scalar *d* denotes the distance separating the actual integration points. Further details can be found in [4]. It is worthwhile noting that (5) must be evaluated numerically and that (5) represents a more general description of the covariance than that one given in [2]. This can be shown using the small argument approximation of the integral kernel in (5), cf. [4].

For the variances the integration collapses and an analytical formulation was obtained, cf. [4]

$$\left\langle \varphi^2 \right\rangle = \frac{12}{5} \frac{0.033}{\Gamma\left(\frac{5}{6}\right)} \frac{\sqrt{\pi^3}\,\kappa_0^{-2/3} 2^{-1/3}}{(\sin\varepsilon)^2} C_n^2 H^2 \left\{ \frac{\pi 2^{1/3}}{\sqrt{3}\,\Gamma\left(\frac{2}{3}\right)}\ {}_2F_3\left(\left[\frac{1}{2},1\right],\left[\frac{2}{3},\frac{3}{2},1\right],\frac{z^2}{4}\right) - \frac{27}{80} 2^{2/3} \Gamma\left(\frac{2}{3}\right) z^{2/3}\ {}_1F_2\left(\left[\frac{5}{6}\right],\left[\frac{11}{6},\frac{7}{3}\right],\frac{z^2}{4}\right) \right\}, \tag{6}$$

where F denotes the hypergeometric function [5]. The dimensionless argument z is given by $z = p\kappa_0 H / \sin\varepsilon$, where the factor p describes the impact of anisotropy on the variance cf. [4] for further details.

With (5) and (6) a new structure for a VCM is provided that describes the impact of turbulent fluctuations of the refractivity on the phase observations. Consequently, this VCM can be interpreted as the VCM for tropospheric delays. Without loss of generality the results can be adopted for the VLBI or INSAR configuration. This VCM gives many insights for the understanding of physical correlations between GNSS phase measurements, some of them are discussed in [4]. In the following section we will focus on the impact of the wind velocity and direction on the VCM.

IMPACT OF THE WIND VELOCITY AND DIRECTION ON THE VARIANCE-COVARIANCE MATRIX

The wind velocity and direction are introduced in the model (2) by (3) to transform the temporal separation of GNSS phase observations into a corresponding spatial separation using Taylor's hypothesis of frozen turbulence. From (5), it is obvious that the magnitude of the covariance and consequently the correlation between two GNSS phase observations (or tropospheric delays) are determined by the separation distance d between the corresponding rays or wavefronts, cf. [4]. Besides the differences in the vectors of lines-of-sight ($\mathbf{r}_B^j - \mathbf{r}_A^i$) and the (possible) station separation ($\boldsymbol{\rho}_A^B$), the distance due to the temporal spacing of the observations ($\mathbf{v}\,\Delta t$) has to be taken into account in (3). If we considered an arbitrary but fixed common height of both integration points (e.g. 1 km), we can evaluate the distance d and its evolution over the time. In particular, we can analyse the contribution of each of the components of **d** to the final distance.

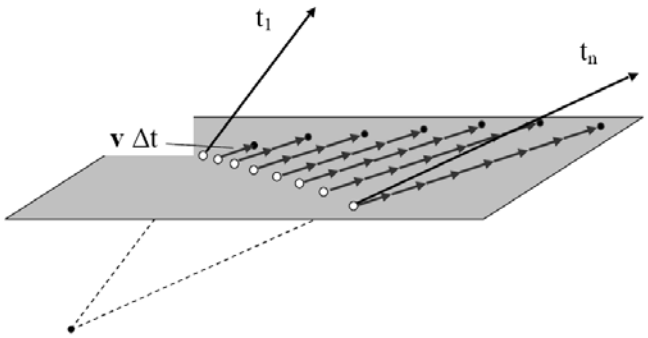

Fig.1. Illustration of the geometric and atmospheric contribution to the separation distance

Fig. 1 shows such a situation for one station and one satellite. We are now interested in the temporal evolution of the separation distance between to distinct epochs t_1 and t_n. The white circles indicate the intersection of the lines-of-sight vectors at each epoch with the plane in constant height. The epochs are assumed to be equidistant.

For the temporal separation $\Delta T = t_i - t_1$ between the first observation and an observation at epoch t_i, the distance between the first white circle and the ith circle represents the *geometric contribution* to the separation distance which is due to the satellite movement on its orbit. For any temporal variation $\Delta T = t_k - t_m$ the corresponding geometric contribution can be represented by the distance between the kth and mth white circle.

Please note that the geometric contribution changes non-uniformly over time. This is due to the different velocities of the satellites on its orbit: the minimum is reached near the zenith and maximum velocities are obtained at low elevation angles. These velocity differences are here reinforced by our representation on a plane at a constant height. In conclusion, for a given time interval Δt minimum geometric contributions are obtained at the zenith. They increase non-uniformly with decreasing elevation angles and leads to maximum geometric contributions at low elevation angles. We can easily extend these geometric considerations to more than one station and one satellite.

In a second step, the wind velocity is considered by superimposing the geometric and the *atmospheric contribution*. This second part is motivated by Taylor's hypothesis of frozen turbulence that assumes that the turbulent structure

travels with a constant horizontal velocity over the region. The atmospheric contributions is parameterized by the product of the wind vector with the temporal separation $\mathbf{\Lambda} = \mathbf{v}\,\Delta t$. In Fig. 1 the corresponding contributions for a unique given time interval Δt are represented by the black arrows. The vector addition leads to the black circles, which indicate the virtual intersection points which should be used for the computation of the separation distance.

Depending on the wind direction, the superposition of both contributions can increase or reduce the values of the separation distance compared to that one obtained from the geometric considerations only. In case of Fig.1 an additive superposition is obtained. In addition, the separation distance changes now more uniformly with time.

A rough estimate of the possible magnitudes of the different contributions (geometric contribution including station separation and the atmospheric contribution) shows that even for moderate wind velocities of some m/s, the atmospheric contribution quickly dominates the total separation distance. Consequently the wind velocity - in combination with the wind direction – governs the correlation and decorrelation process which will be shown in the following.

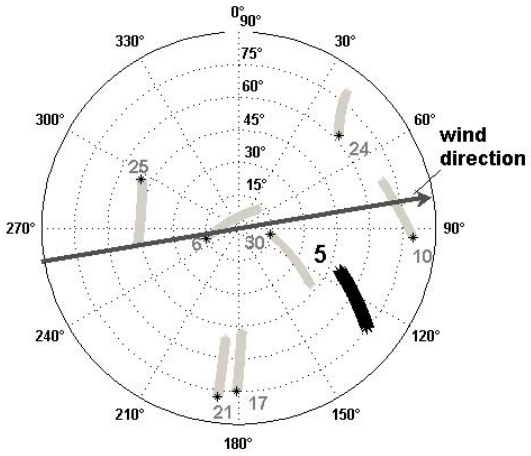

Fig.2 skyplot

In order to show how these effects are represented in our VCM model, we simulate the values of the VCM for an one hour segment with a sampling rate of 1 s for a real satellite configuration. We consider two basic scenarios: (S1) no wind velocity is applied and (S2) a wind velocity of 4 m/s in the azimuth A =80° is applied. The parameter values used for the structure constant, outer scale length, etc, are reported in [4]. The skyplot for the resulting 3600 epochs is shown in Fig. 2. The satellites are numbered by their PRN codes and the asterix indicates the starting point during the 1 h segment. In addition, in Fig. 2 the wind direction is indicated.

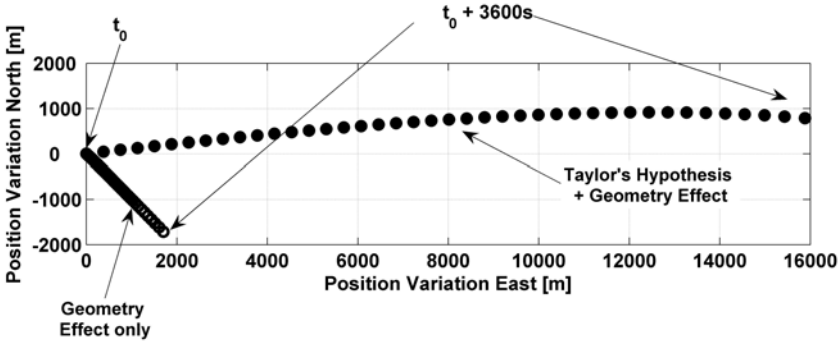

Fig. 3. Comparison of the separation distances for both scenarios for the PRN5

In the following we focus on the satellite PRN5. Fig. 3 shows the variations of the intersection points in a horizontal plane at 1 km height for both scenarios: For S1 only the geometric contribution is realised which leads to short separation distances between the observations. Consequently high covariances and correlations between the observations will be obtained. For S2 the atmospheric contribution is superimposed which clearly dominates the length of the final separation distance. Consequently, for long temporal separations the covariances are very small, and the observations are completely decorrelated which reflects more realistically the actual behaviour.

(a) (b)

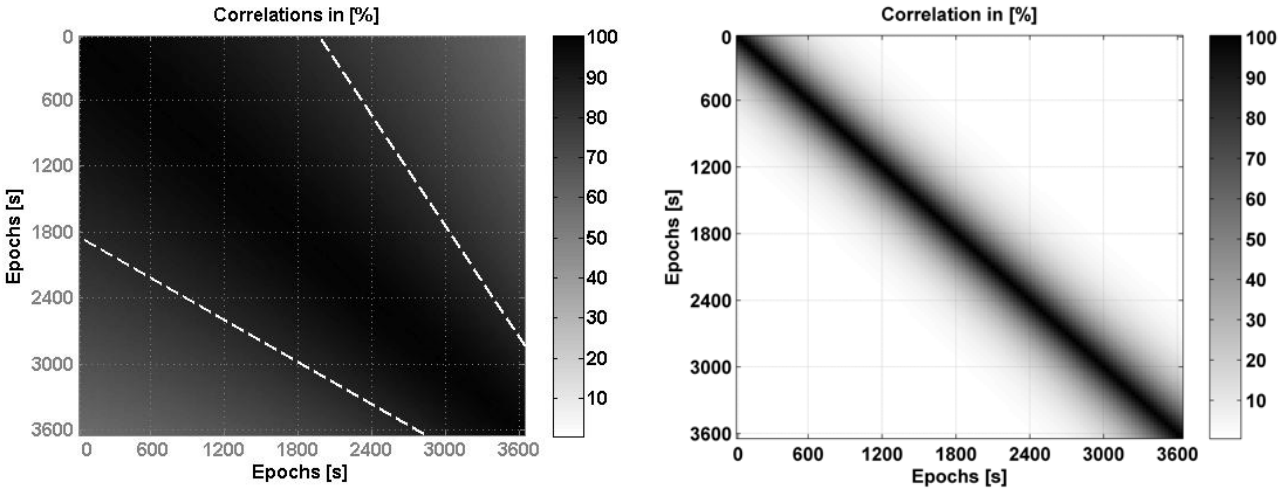

Fig.4. Comparison of the resulting correlation matrices for PRN5, (a) Scenario 1, geometric contribution only, (b) Scenario 2, superposition of geometric and the atmospheric contribution.

Fig. 4 compares this impact for the 3600 x 3600 correlation matrix of the observations. Fig. 4(a) shows the results for scenario S1 (geometric contributions only), Fig. 4(b) the results for S2 (superposition of atmospheric and geometric contributions). Dark grey values indicate strong correlations. The white dashed lines in Fig. 4(a) are added to emphasize the non-uniformity of the increase of the separation distance for the considered setting satellite PRN5. At the beginning of the exemplary 1 h segment the satellite PRN5 is at moderate elevation angles (45°) and sets to elevation angles of 15°, cf. Fig.2. At moderate elevation angles, the velocity of the satellite is slower that at low elevation angles yielding shorter separation distances for the same temporal separation interval and hence higher correlations. Consequently, the lines of an equal amount of correlations are not parallel to the main diagonal. In addition due to the small resulting separation distances the overall correlation level is unrealistically high. The correlations are rarely smaller than 50%, even for long temporal separations of 3600s.

In Fig. 4(b) the situation completely changes. Much larger separation distances lead to a decorrelation of consecutive observations after about 300 s. The geometry of the setting satellite is no longer reflected in the correlation matrix since the separation distances are dominated by the atmospheric contribution which is uniform over time, i.e. the lines of equal amount of correlations are parallel to the main diagonal. Finally this diagonal structure is mathematically easier to handle. This is a non-neglectable advantage for the necessary matrix inversion during the data analysis steps and parameter estimation procedures by a least-squares adjustment.

CONCLUSIONS AND OUTLOOK

In this paper, we summarized our development based on turbulence theory of variances and covariances of space-geodetic phase observations (VLBI or GNSS carrier phase observations) that adequately assess refractivity fluctuations in the troposphere. The obtained fully populated VCM of the observations is a generalisation of the model given by [2]. Furthermore it can be interpreted as the VCM for the slant tropospheric delays. In a second part, it was shown that the wind velocity and direction play a key role for the structure of the VCM and the associated correlation matrix. In fact, the atmospheric contribution dominates the values of the separation distance between the observations yielding a strong decorrelation of the phase observations and a tri-diagonal structure of the VCM.

The comparison of the correlations predicted be the model (5) and (6) and empirical auto- and cross-correlation functions is investigated in [3]. Using the double-differenced GPS phase data from a specially designed network, a good agreement between the empirical auto- and cross-correlations functions and the correlation obtained from the model is found when using the geostrophic wind which can be easily computed from isobaric maps. Consequently, the new VCM (5,6) adequately models physical correlations and covariances that are induced by refractivity fluctuations in the troposphere.

The development of new GNSS such as Galileo will on the one hand contribute to enhance the temporal and spatial repeatability of the satellite passes and therefore improve the troposphere sensing and understanding the complex processes in the troposphere. On the over hand for high precision application and for a meaningful interpretation and validation of the estimated parameters physical correlations between the GNSS observations cannot be neglected any longer. Consequently, an extended variance-covariance model such as the one proposed in this paper should be implemented.

ACKNOWLEDGEMENT

This paper presents ideas which were developed as part of the Feodor-Lynen-Fellowship (2004-2006) of the first author at the Institute for Engineering Geodesy and Measurement Systems of the Graz University of Technology with Fritz K. Brunner as his host. He gratefully thanks the Alexander von Humboldt-Foundation for the support.

REFERENCES

[1] A.D. Wheelon, *Electromagnetic Scintillation – I. Geometrical Optics*, Cambridge: Cambridge University Press, 2001.

[2] R.N. Treuhaft, G.E. Lanyi, “The effect of the dynamic wet troposphere on radio interferometric measurements”, Radio Sci ,vol.22(2), pp. 251-265 1987

[3] S. Schön, F.K. Brunner, “A proposal for modelling physical correlations of GPS phase observations”, J Geod (in review) 2007

[4] S. Schön, F.K. Brunner, “Atmospheric turbulence theory applied to GPS phase data”, J Geod (in press) 2007

[5] M. Abramowitz, I.A. Segun, *Handbook of mathematical functions*. New York: Dover, 1972.